Neutron star pulse profiles in scalar-tensor theories of gravity

Hector O. Silva and Nicolás Yunes

Neutron star pulse profiles in scalar-tensor theories of gravity

Hector O. Silva[1, *] and Nicolás Yunes[1, †]

[1]eXtreme Gravity Institute, Department of Physics, Montana State University, Bozeman, Montana 59717 USA

The observation of the x-ray pulse profile emitted by hotspots on the surface of neutron stars offers a unique tool to measure the bulk properties of these objects, including their masses and radii. The x-ray emission takes place at the star's surface, where the gravitational field is strong, making these observations an incise probe to examine the curvature of spacetime generated by these stars. Motivated by this and the upcoming data releases by x-ray missions, such as NICER (Neutron star Interior Composition Explorer), we present a complete toolkit to model pulse profiles of rotating neutron stars in scalar-tensor gravity. We find that in this class of theories the presence of the scalar field affects the pulse profile's overall shape, producing strong deviations from the General Relativity expectation. This finding opens the possibility of potentially using x-ray pulse profile data to obtain new constraints on scalar-tensor gravity, if the pulse profile is found to be in agreement with General Relativity.

I. INTRODUCTION

Neutron stars are some of the most extreme objects in the Universe, and thus, they serve as a unique laboratory to probe fundamental physics. Their large masses ($m \approx 1.4\,M_\odot$) combined with their small radii ($R \approx 12$ km) result in supranuclear densities at their cores, whose description challenges our current understanding of matter. The latter is encoded in the star's equation of state, whose determination is an outstanding problem in nuclear astrophysics [1]. Moreover, the strong gravitational fields produced by neutron stars result in gravitational potentials $\sim Gm/(Rc^2)$ that are nine orders of magnitude larger than what we can probe on Earth's surface [2, 3]. Therefore, to correctly describe these stars, we must rely on a relativistic theory of gravity [4].

The leading theory is of course Einstein's theory of General Relativity. During its centennial existence, the theory has shown a remarkable predictive power, being consistent within all experimental tests carried out so far, ranging from local, Solar System experiments [2], to the spectacular detection of gravitational waves by the LIGO/Virgo collaboration [5, 6]. This consistency with observation is even more striking when one notes that the theory (unlike most of its alternatives) does not possess any free parameters that can be tuned to make its predictions agree with Nature.

Given the success of General Relativity, why should we even consider modifications to it and examine their observational consequences? The reasons are many, but they can be organized in two main classes [7–9]. On the observational front, the late time expansion of the Universe [10, 11], the rotation curve of galaxies [12, 13], the baryon-anti-baryon asymmetry [14, 15], and other cosmological observations seem to point at either exotic dark fluids or modifications to General Relativity. On the theoretical front, the incompatibility of General Relativity with quantum mechanics has prompted many attempts at extensions, from string theory to loop quantum gravity and other variations.

Can neutron star observations[1] be used to learn about gravity in extreme environments? A general prediction of modified theories of gravity is that the bulk properties of the star (e.g. its radius and mass) are different from those predicted by General Relativity. Tests of gravity in this direction are however limited by a strong degeneracy problem between the equation of state and the gravity theory: the modifications of the bulk properties of these stars caused by changes in the gravitational theory are (often) degenerate with modifications due to different equations of state [26].

One option to bypass this issue is to focus on electromagnetic phenomena in the vicinity of neutron stars [27]. These phenomena include e.g. atomic spectral lines [28], burst [29, 30] and quasiperiodic oscillations [30–33]. One can argue that in these scenarios one can in principle probe the *exterior spacetime* of the star, offering a glimpse on possible deviations from General Relativity, without worrying about the intricacies of the stellar interior.

The observation of x-ray waveforms or pulse profiles from rotating neutron stars is another potentially interesting phenomenon to consider [34]. In this scenario, a region of of the neutron star's surface becomes hot (relative to the rest of the star's surface) generating an x-ray flux modulated by the star's rotation. This *hotspot* can be formed in a number of situations (see [35–37] for reviews). In accretion-powered pulsars, material is channeled through the magnetic field lines and heats the star up when it reaches its magnetic poles. In burst oscillations, a thermonuclear explosion caused by infalling matter results in a hotspot on the surface of the accreting neutron star. In all these cases, the modeling of the resulting waveform, combined with x-ray observations, allows for the extraction of a number of properties of the source, including the neutron star's mass and radius, see e.g. [38–47].

The ongoing NICER (Neutron star Interior Composition Explorer) mission [48–50] offers a substantial improvement over the preceding x-ray observatory, the Rossi X-ray Timing Explorer (RXTE), opening the path to measurements of

---

* hector.okadadasilva@montana.edu
† nicolas.yunes@montana.edu

---

[1] We here focus on properties of *individual* stars. Neutron stars have already proven invaluable tools to constrain deviations of General Relativity when either in binaries [16–18] (or triple [19]) systems or more recently binary neutron stars mergers [20] (see e.g. [21–25]).

stellar masses and radii with unprecedented accuracy – with immediate implications to our understanding on the neutron star equation of star. Given, the scientific potential of NICER, it is natural to ask: *can we use its observations to probe the strong-field regime of gravity*? In this paper, we take the first necessary steps to find an answer to this question. We find hints that NICER can indeed be used to probe the strong-field regime of gravity, but a definite answer will require a plethora of theoretical and data analysis work that this paper now enables (see [51, 52] for independent recent work in this direction).

A. Executive summary

We present a complete toolkit to model the x-ray flux from radiating neutron stars in scalar-tensor gravity, one of the most well-studied and well-motivated extensions of General Relativity [53, 54]. This class of theories extends General Relativity by introducing a scalar field that couples to the metric nonminimally, thus violating the strong-equivalence principle. Our formalism and the resulting toolkit are completely model-independent within this class of scalar-tensor theories. Moreover, the resulting waveforms include Doppler shifts, relativistic aberration and time-delay effects, thus extending [52]. All of these effects are critical ingredients that are necessary to develop an accurate pulse-profile model, and thus, our toolkit now enables a complete data analysis study that will be carried out in the future.

Figure 1 shows a sample waveform that takes all the previously mentioned effects into account, illustrating the difference between the predictions of both theories. As will discuss in Sec III, we find that the presence of the scalar field influences the exterior spacetime of the neutron star, altering the bending of light and the time-delay experienced by photons emitted by the star. The net result of these contributions is a waveform that can be considerably different in comparison to General Relativity's predictions. Such a model now enables, for the first time, a serious data analysis investigation of whether such waveform differences can be detected/constrained with data or whether they are degenerate with other waveform parameters.

The remainder of this paper is organized as follows. In Section II, we briefly review the basic of scalar-tensor gravity, discussing the properties of the exterior spacetime of neutron stars in this theory. Next, in Section III, we present in detail how we construct our pulse profile model. Finally, in Section IV we show a few examples of the pulse profile of burst oscillations and discuss the modifications introduced by scalar-tensor gravity. We discuss in details the roles played by different effects on the overall shape of the resulting waveform. We close with Section V, summarizing our main findings and discussing some possible extensions and applications of this work.
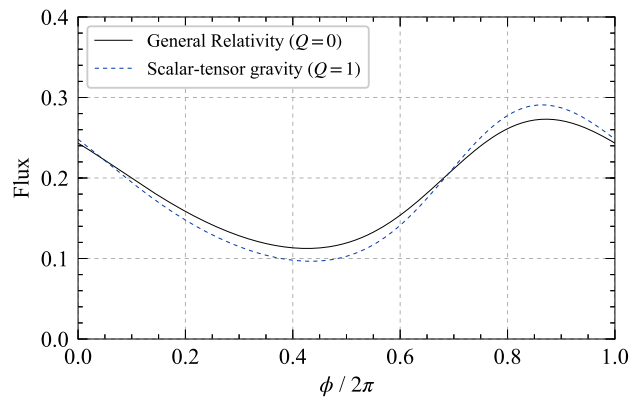

FIG. 1. An illustrative bolometric flux for a single hotspot over one revolution of the rotating neutron star in General Relativity and scalar-tensor gravity. The star has $u \equiv 2G_* m/(Rc^2) = 0.5$ and mass $m = 1.4 \, M_\odot$ in both cases. The only difference between the two models is the presence of a nonzero scalar charge for the star in scalar-tensor gravity. The magnitude of the scalar charge is quantified by the scalar charge-to-mass ratio Q (described in Sec. II) which is zero in General Relativity and controls by how much the spacetime is different from the usual Schwarzschild spacetime. This particular examples a sample star labeled c_3 as discussed in Sec. II (cf. Table I).

II. OVERVIEW OF SCALAR-TENSOR THEORY

A. Action and field equation

Scalar-tensor theories are one of the most widely studied and well-motivated extensions to General Relativity. In this class of metric theories of gravity, the gravitational interaction is mediated by an additional scalar field φ. Assuming this scalar field to be long-ranged (i.e. massless), the theory can be described by an action S_* in the so-called Einstein frame given by [55]:

$$S_* = \frac{c^4}{4\pi G_*} \int \frac{d^4x}{c} \sqrt{-g_*} \left[\frac{1}{4} R_* - \frac{1}{2} g_*^{\mu\nu} \nabla_\mu \varphi \nabla_\nu \varphi \right] + S_m[\psi_m, g_{\mu\nu}], \tag{1}$$

where c is the speed of light in vacuum, and G_* is the bare Newtonian constant. The action is written in terms of the Einstein frame metric $g_{*\mu\nu}$, with metric determinant $g_* \equiv \det[g_{*\mu\nu}]$ and Ricci curvature scalar R_*. Matter fields, collectively represented by ψ_m, are minimally coupled to the Jordan frame metric $g_{\mu\nu} \equiv A^2(\varphi)g_{*\mu\nu}$, with $A(\varphi)$ being a conformal factor. As such, clocks and rods in the real world measure time intervals and distances of $g_{\mu\nu}$ and not of $g_{*\mu\nu}$. The advantage of working in the Einstein frame is that the field equations are simpler, making it technically easier to derive predictions for the theory. However, in the end, we will express the relevant observables in the Jordan frame.

The field equations, obtained by varying Eq. (1) with re-

spect to $g_*^{\mu\nu}$ and φ, are:

$$R_{*\mu\nu} = 2\partial_\mu\varphi\partial_\nu\varphi + \frac{8\pi G_*}{c^4}\left(T_{*\mu\nu} - \frac{1}{2}T_* g_{*\mu\nu}\right), \qquad (2)$$

$$\Box_*\varphi = -\frac{4\pi G_*}{c^4}\alpha(\varphi)T_*, \qquad (3)$$

where $T_*^{\mu\nu} \equiv (2c/\sqrt{-g_*})(\delta S_{\mathrm{m}}/\delta g_{*\mu\nu})$ is the Einstein frame energy-momentum tensor and $T_* \equiv g_*^{\mu\nu}T_{*\mu\nu}$ is its trace. The energy-momentum tensor acts as a source for the scalar field, through the coupling $\alpha(\varphi) \equiv \mathrm{d}\log A(\varphi)/\mathrm{d}\varphi$. The choice of $A(\varphi)$ determines a specific scalar-tensor theory and a number of models have been studied in the literature.

From the definition of $T_{*\mu\nu}$, one can derive the following expressions that connect the Einstein and Jordan frame energy-momentum tensors (and their traces):

$$T_{\mu\nu} = A^2(\varphi)T_{*\mu\nu}, \quad T^{\mu\nu} = A^{-6}(\varphi)T^{*\mu\nu}, \quad T = A^{-4}(\varphi)T_*. \quad (4)$$

Finally, the covariant divergences of $T_*^{\mu\nu}$ and $T^{\mu\nu}$ read:

$$\nabla_{*\mu}T_*^{\mu\nu} = \alpha(\varphi)T_*\nabla_*^\nu\varphi, \qquad \nabla_\mu T^{\mu\nu} = 0. \qquad (5)$$

B. Exact exterior neutron star spacetimes

The pulse profile of a radiating neutron star depends on its *vacuum exterior* spacetime. In General Relativity, the exterior spacetime of a static, spherically symmetric star is described by the Schwarzschild metric (by Birkhoff's theorem), whose line element is

$$\mathrm{d}s_{\mathrm{Sch}}^2 = -f_{\mathrm{Sch}}\,\mathrm{d}(ct)^2 + f_{\mathrm{Sch}}^{-1}\,\mathrm{d}r^2 + r^2\mathrm{d}\Omega \qquad (6)$$

in Schwarzschild coordinates (t, r, θ, ϕ). In this equation, $\mathrm{d}\Omega = \mathrm{d}\theta^2 + \sin^2\theta\,\mathrm{d}\phi$ is the line element on a unit-sphere and the Schwarzschild factor is defined via

$$f_{\mathrm{Sch}} \equiv 1 - 2Gm/(c^2 r), \qquad (7)$$

with G Newton's gravitational constant, and m the gravitational mass of the star. Thus, the metric is entirely determined by the mass of the star.

In scalar-tensor gravity, the exterior spacetime of a static, spherically symmetric star sourcing a nontrivial scalar field in the Einstein frame is given by the Just spacetime [55–58]:

$$\mathrm{d}s_*^2 = -f^{b/a}\mathrm{d}(ct)^2 + f^{-b/a}\mathrm{d}\rho^2 + \rho^2 f^{1-b/a}\mathrm{d}\Omega \qquad (8)$$

in Just coordinates (t, ρ, θ, ϕ) [57]. In this equation, $\mathrm{d}\Omega$ is still the line element on an unit-sphere, $b \equiv 2G_* m/c^2$, but now

$$f \equiv 1 - \bar{a}. \qquad (9)$$

with $\bar{a} \equiv a/\rho$ and a a real constant with units of length that is related to both the mass of the star m and the strength of the scalar field. The transformation relating Just and Schwarzschild coordinates is given by [55]

$$r = \rho(1 - \bar{a})^{(1-b/a)/2}. \qquad (10)$$

but this expression is not analytically invertible. Therefore, the Just line element in Just coordinates cannot in general be transformed to Schwarzschild coordinates analytically, although it can be done numerically. The Just line element in the Jordan frame is related with (8) as $\mathrm{d}s^2 = A^2(\varphi)\mathrm{d}s_*^2$.

The scalar field configuration sourced by the star has the form

$$\varphi = \varphi_\infty + (q/a)\log(1 - \bar{a}). \qquad (11)$$

Far from the star ($\bar{a} \ll 1$), $\varphi \simeq \varphi_\infty - q/\rho$ and therefore, q is the scalar charge of the star, while φ_∞ is the cosmological background value of φ, which we assume to be zero[2]. We also assume that the conformal factor is such that $A(\varphi_\infty) = 1$ asymptotically. As a consequence, the Einstein and Jordan-frame masses are the same $m = m_*$ [63, 64]. Additionally the gravitational constant measured in the weak-field regime in a Cavendish experiment is $G = A^2(\varphi_\infty)\,G_*[1 - \alpha(\varphi_\infty)^2]$.

The exterior spacetime of a neutron star in scalar-tensor theories is therefore determined not just by the star's mass m (or equivalently b), but also by the parameters q and a. These constants, however, are not all independent. Instead, they obey the constraint

$$a^2 - b^2 - (2q)^2 = 0. \qquad (12)$$

We can use this relation to elucidate the meaning of the ratio a/b present in Eq. (8):

$$a/b = \sqrt{(2q/b)^2 + 1} = \sqrt{1 + Q^2} \qquad (13)$$

where we used $b = 2G_* m/c^2$ to define a dimensionless scalar charge-to-mass ratio

$$Q \equiv qc^2/(G_* m). \qquad (14)$$

The exterior spacetime is therefore fully determined by the pair (m, Q), with Q controlling the departure from the Schwarzschild spacetime, which is recovered when $Q = 0$ (and thus $a/b = 1$).

C. Constraints on scalar-tensor theories and the parameter space of neutron star models

In practice, few direct observational constraints on the scalar charge-to-mass ratio Q exist. In [65], Horbatsch and Burgess developed a conformal factor $A(\varphi)$ and equation-of-state-independent framework which can be used to directly constrain Q if a sufficient number of post-Keplerian parameters are known from a binary system. When applied to the binaries PSR J0737-3039A/B and PSR B1534+12 they obtained the upper bounds $|Q| = 0.21$ and $|Q| = 0.44$ (at 68% confidence level) respectively. We use the latter value to guide

---

[2] Rigorously, the present day value of φ_∞ has to be determined from the cosmological evolution of the theory [59–62].

an estimate of the largest magnitude of Q allowed from observations; for concreteness we use $Q = 0.5$.

The parameter Q, is also constrained by theoretical considerations. Clearly, for any given equation of state, if the compactness is large enough, the neutron star will collapse and form a black hole (see [66, 67] for studies in particular scalar-tensor gravity models). An estimate of this compactness was found by Buchdahl [68, 69] in General Relativity [$Gm/(Rc^2) < 4/9$]. Extending this work to scalar-tensor theories, Tsuchida et al. [70] found that in the Einstein frame, a, b and q have their values bounded under a minimal set of assumption akin to those of Buchdahl [69]: that the star is a perfect fluid, that the density is positive (and monotonically decreasing) and that the solution matches the Just metric at the star's surface.

We can write this constraint on Q differently by working directly with the parameters a and b from Eq. (13). With this reparameterization, the result from [70] delimits a domain $\mathcal{D}$ (in a plane spanned by $\bar{a}_s = a/\rho_s$ and $\bar{b}_s \equiv b/\rho_s$, where ρ_s is the star's radius in Just coordinates) given by:

$$\bar{b}_s \leq \bar{a}_s \leq 2\sqrt{\bar{b}_s} - \bar{b}_s \,, \text{ for } 0 \leq \bar{b}_s \leq 4\left(3 - 2\sqrt{2}\right)$$

$$\bar{b}_s \leq \bar{a}_s \leq 2\left(\sqrt{2\bar{b}_s} - \bar{b}_s\right), \text{ for } 4\left(3 - 2\sqrt{2}\right) \leq \bar{b}_s \leq 8/9$$

$$\text{no stars exist}\,, \text{ for } \bar{b}_s > 8/9 \qquad (15)$$

in which the theory [for any given $A(\varphi)$] admits stellar solutions. We can thus use these inequalities as a guide to select neutron star models in scalar-tensor gravity, parametrized by $\bar{a}_s$, $\bar{b}_s$ and A_s, *irrespective* of the equation of state of the stellar interior and of the conformal factor $A(\varphi)$. This makes our analysis *as model-independent as possible*.

The domain $\mathcal{D}$ is shown by the shaded region in Fig. 2. The left panel shows the inequalities in Eq. (15), while in the right panel we re-express them in terms of $a/b = \bar{a}_s/\bar{b}_s = \sqrt{1 + Q^2}$ instead of $\bar{a}_s$. For reference, we also shows lines of constant Q, with the solid line corresponding to General Relativity with $Q = 0$. Black holes are shown by the point labeled $\mathcal{S}$, while "Newtonian" solutions (with very small compactness) are at the origin of the plane (left-panel) or toward the left-end (right-panel). In virtue of the no-hair theorem of Sotiriou and Faraoni [71], black holes have zero scalar charge $q = 0$ (thus $Q = 0$, $a = b$) and compactness $u/2 = G_*m/(Rc^2) = 0.5$ in theories described by the action in Eq. (1).

The hatched portion of the plane *qualitatively* represents the region in which neutron stars could exist. Assuming small deviations from General Relativity (i.e. small Q as justified previously), we expect the conformal factor evaluated at the star's surface to be of order unity $A_s \equiv A[\varphi(\rho_s)] \approx 1$, hence $R \approx \rho_s$, where R is the circumferential, Jordan-frame radius of the star. Astronomical observations show that neutron stars have masses approximately in the $m \in [0.9, 2.0]$ $M_\odot$ and radii $R \in [8, 14]$ km ranges, which translate into $u \approx b_s \in [0.19, 0.74]$ [72, 73]. Therefore, the region between the general relativistic solutions and the constant $Q = 0.5$ line delimits the region where neutron stars could exist.

An additional region of interest arises from studying when the photon light ring (or light rings) of the Just metric is inside

the radius of the star. This allows a photon emitted tangentially from the surface of the star to reach the observer [74]. Otherwise, if the light ring is outside of the star, then tangential photons would come back to hit the surface, and thus, they would not reach the observer. In Appendix A, we show that this occurs when

$$\bar{a}_s \leq 2(1 - \bar{b}_s)\,, \quad \text{or} \quad (\bar{b}_s/2)(2 + \sqrt{1 + Q^2}) \leq 1\,, \qquad (16)$$

which is shown by dash-dotted lines in Fig. 2.

Due to the large parameter space available for stellar models in scalar-tensor gravity we must make a few sensible requirements for choosing our illustrative stellar models. All stars in our catalog: (i) obey the constraints (15); (ii) have a canonical mass of $m = 1.4\ M_\odot$; (iii) have twice the compactness of $u = \{1/3, 1/2\}$ [3]. In this way, our stellar models in scalar-tensor gravity are "doppelgängers" of their general relativistic models counterparts: they have the same gravitational mass m and (Jordan-frame) areal radius R – the only difference being the presence of a nonzero scalar charge. Although we expect $A_s \approx 1$, there is no particular reason to chose it either larger or smaller than unity – we thus consider both possibilities.

Under these choices we group them in three classes according to their value of Q.

- Models a_i represent general relativistic stars ($Q = 0$).

- Models b_i represent stars with $Q = 0.5$. To determine ρ_s we assume that the conformal factor evaluated at the surface A_s is 1.0 ± 0.05.

- Models c_i represent stars with $Q = 1.0$. To determine ρ_s we assume that A_s is 1.0 ± 0.1.

The parameters of these stellar models are listed in Table I. Given the constraint on $|Q|$ [65], why should we consider values as large as unity? The reasons are two-fold. First, regardless of the constraint, it is of theoretical interest to investigate how much (and precisely how) this new parameter affects the pulse profile. This question cannot be answered if we restrict ourselves to $Q \approx 0$. Second, if it were the case that even for a maximal value of Q in the range of reasonable values (say even for $Q = 1$), the impact of the scalar charge on the pulse profile is minimal, then there would little motivation to attempt to constraint this theory using pulse profile observations.

D. Connection to specific scalar-tensor gravity models

Although our discussion so far has been fully model-independent, one can easily determine the parameters (m, Q) within a specific scalar-tensor model. We here briefly explain

---

[3] These are illustrative values used by Poutanen et al. [75] which we will use to validate the numerical implementation of our pulse profile code in Sec. IV
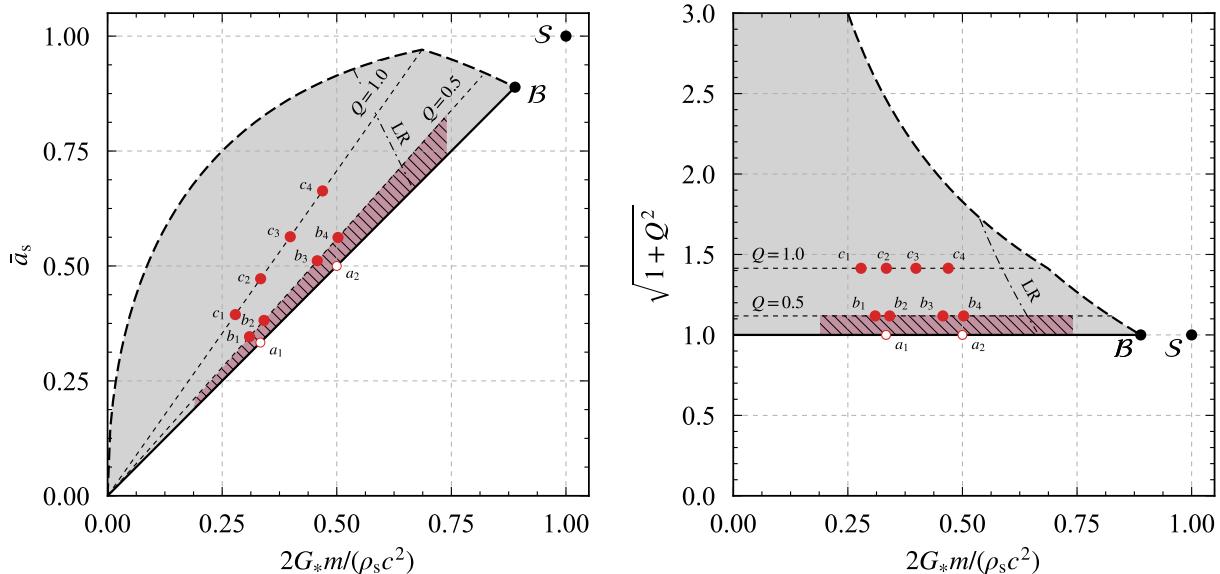
FIG. 2. The existence domain $\mathcal{D}$ of stars in scalar-tensor theories parameterized in terms of $\bar{a}_s$ and $\bar{b}_s [= 2G_* m/(\rho_s c^2)]$ (left panel) and in terms of Q and $\bar{b}_s$ (right panel). Stellar solutions exist within the shaded regions of both panels. General relativistic stars lay on the solid line $\bar{a}_s = \bar{b}_s$ and $Q = 0$, with Newtonian configurations located near the origin of the plane in the left panel and near the left end in the right panel. Buchdahl's limit terminates these lines at the point $\mathcal{B} = (8/9, 8/9)$ in the left panel and $\mathcal{B} = (1, 8/9)$ in the right panel, while black holes are located at the point $\mathcal{S} = (1, 1)$ in both panels. Moving away from general relativistic line, we enter the realm of stars in scalar-tensor gravity ($Q \neq 0$). Their existence is bound from above by the inequalities in Eq. (15) (dashed curve). The dashed-dotted line (labeled "LR") correspond to the light ring location given by Eqs. (16).

Name	u	$m/M_\odot$	R/km	ρ_s/km	A_s	$\bar{a}_s$	$\bar{b}_s$	Q
a_1	0.333	1.4	12.40	12.40	1.00	0.333	0.333	0.0
a_2	0.500	1.4	8.269	8.269	1.00	0.500	0.500	0.0
b_1	0.333	1.4	12.40	13.35	0.95	0.346	0.309	0.5
b_2	0.333	1.4	12.40	12.12	1.05	0.381	0.341	0.5
b_3	0.500	1.4	8.269	9.040	0.95	0.511	0.457	0.5
b_4	0.500	1.4	8.269	8.227	1.05	0.562	0.503	0.5
c_1	0.333	1.4	12.40	14.83	0.90	0.394	0.279	1.0
c_2	0.333	1.4	12.40	12.38	1.10	0.472	0.334	1.0
c_3	0.500	1.4	8.269	10.37	0.90	0.564	0.398	1.0
c_4	0.500	1.4	8.269	8.817	1.10	0.663	0.469	1.0

TABLE I. *Stellar models.* We list the properties of the stellar models which we used to compute the pulse profiles. The parameters are: u (twice the compactness), m (the gravitational mass), R (Jordan-frame radius in Schwarzschild coordinates), ρ_s (Einstein-frame radius in Just coordinates), A_s (conformal factor evaluated at Einstein-frame radius in Just coordinate ρ_s), $\bar{a}_s = a/\rho_s$, $\bar{b}_s = b/\rho_s$, Q (scalar charge-to-mass ratio). The conformal factor A_s is necessary to translate radii between Einstein to Jordan frames.

how this can be done once a specific functional form of $A(\varphi)$ is chosen.

The first step consists of integrating the stellar structure equations of a static, spherically symmetric neutron star in scalar-tensor theory, which generalize the Tolman-Oppenheimer-Volkoff equations from General Relativity. These equations are derived from the field equations [Eqs. (2) and (3)] assuming matter to be described by a perfect fluid. The explicit form of these equations and a description of the numerical algorithm used to integrate them can be found, e.g. in [76–78].

Once a stellar model has been constructed, the quantities q, m, R and A_s are all known. From m, we immediately determine b. Using Eq. (12) we find a, while from Eq. (10) we obtain ρ_s. At last, Q is obtained from Eq. (14). With these values, the Just spacetime is completely determined.

III. PULSE PROFILE MODELING

Having presented an overview of scalar-tensor gravity, the properties of the exterior neutron star spacetime and some generic properties of neutron stars in this theory, we are now ready to develop a pulse profile model. We start with a description of our assumptions, followed by an analysis of geodesic motion in the Just spacetime and we close by constructing the pulse profile model.

A. Assumptions and model parameters

Several models have been developed to study the pulse profile of radiating, rotating neutron stars, since the pioneering

work by Pechenick et al. [74] (see [35–37] for reviews). Given that this is one of the first detailed study of pulse profiles in non-GR theories, we will make a series of simplifying physical assumptions, to be relaxed in future work. In this section, we lay down and justify these assumptions.

(i) *The stellar model, its exterior spacetime and photon geodesics.* We assume a spherically symmetric neutron star described by a solution of the field equations of scalar-tensor theory with a perfect fluid. The exterior spacetime (Sec. II B) is described by two parameters: Q and m. The ratio of a/b determines the scalar charge-to-mass ratio Q [cf. Eqs (13) and (14)]. Photons move on geodesics of the Just spacetime in the Jordan frame (8).

(ii) *Hotspot.* We assume that the star has a small (relative to the size of the star), uniformly-radiating, hotspot on its surface, located at a polar angle θ_s. Analytical estimates [79] and numerical simulations [80] in General Relativity provide evidence that the hotspot size has a small impact on the pulse profile observed, provided the spot is small enough. In reality, the spot size is likely not sufficiently small for this effect to be ignorable, but here, for simplicity, we will assume it to be infinitesimal in size and that the rest of the star is dark, assumptions that can be lifted in the future. We assume that the scalar field does not affect either the process of generation of radiation nor its spectral properties.

(iii) *Rotation and special relativistic effects.* The star rotates with a constant frequency ν and we neglect the effects of frame-dragging on the emitted radiation. These effects have been shown to be small (in General Relativity) and we expect them to be equally small in scalar-tensor gravity [81]. At high rotation frequencies ($\nu \gtrsim 300$ Hz), the pulse profile is mostly affected by the quadrupolar deformation of the star [82–87] which, however, we do not include. However, we do include special relativistic effects of Doppler boost and aberration due to the rapid motion of the hotspot. That is, we work in a "Just-Doppler" approximation, in analogy with the "Schwarzschild plus Doppler" approximation introduced by Miller and Lamb [38] who worked with the Schwarzschild spacetime (see also Refs. [42, 75]).

(iv) *Photon time delay.* Photons emitted at different rotation phases $\phi_s \equiv 2\pi\nu t$ take different paths to reach the observer, resulting in a time-delay Δt (Sec. III D). This time-delay forces the observed phase of the pulse ϕ_{obs} to be shifted with respect to the star's rotational phase as $\phi_{obs} = \phi_s + 2\pi\nu\Delta t$. This effect is only appreciable for fast rotators: for a rotational period of $P = 1.5$ ms, this induces at most a 5% correction to the photon arrival phase in General Relativity [75]. We do include this effect for completeness.

(v) *Observer.* The observer is located a distance D from the star, at an inclination ι_o relative to the star's rotation axis. We express the physical observables in the
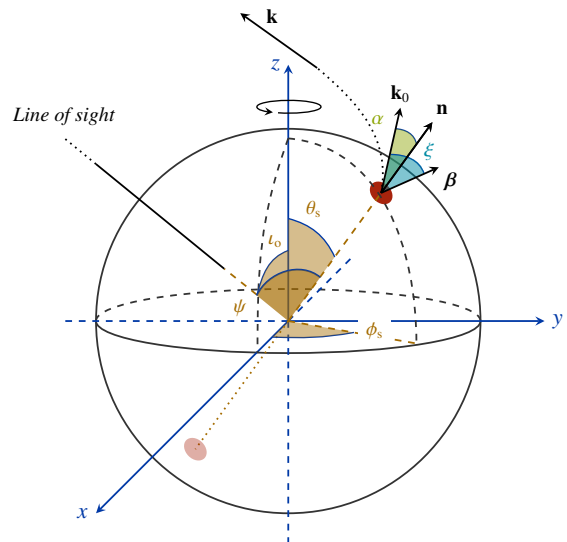

FIG. 3. Geometry of a rotating neutron star with hotspots. The star is here depicted as rotating about the positive z axis, with two antipodal hotspots in red, and a variety of angles defined in the text. The line of sight and the vector k lay on the same plane which passes by the origin on the figure.

Jordan frame, which are the quantities measured by the observer's rods and clocks.

The geometry of the problem is depicted in Fig. 3. The hotspot is located at the stellar surface at polar angle θ_s and its instantaneous position is described by a radial unit vector n. The unit vector n and the line of sight make an angle ψ. The trajectory of emitted photons can be described by a unit vector k_0, which makes an angle α with respect to the normal n. We are interested in the photons whose trajectories (after experiencing gravitational light bending) are along the line of sight of the observer. These photon trajectories are depicted by the unit vector k. Finally, β is a vector, perpendicular to n and tangential to the (instantaneous) direction in which the hotspot moves. We denote by ξ its angle with respect to k_0. When present, an antipodal hotspot is located at $\theta = \pi - \theta_s$ and $\phi = \pi + \phi_s$.

With this at hand, the plan for the remainder of this section is as follows: (i) to study geodesic motion in the Just spacetime to obtain a relationship between the angles ψ and α, which will tell us which photons reach the observer, and (ii) to obtain relations for the angles ι_o, θ_s, ϕ_s, α and ξ which we will use to construct the flux measured by the observer, including special relativistic effects caused by the rapid motion of the hotspot.

B. Null geodesic motion in the Just spacetime

To construct the bolometric flux measured by an observer, the first step is to analyze the photon's geodesic motion in the

Just metric. In particular, the goal of this section is to obtain an expression for the angle ψ, shown in Fig. 3.

We define the Lagrangian

$$L = g_{\mu\nu} p^\mu p^\nu, \qquad (17)$$

where the photon's Jordan-frame four-momenta is defined as $p^\alpha \equiv dx^\alpha/d\lambda$ [with $x^\mu = (ct, \rho, \theta, \phi)$ the four-trajectory of the photon], where λ is an affine parameter.

Because of spherical symmetry, the photon geodesic is confined to a constant θ-plane, which we take to be the equatorial plane ($\theta = \pi/2$). Using the line element in Eq. (8) to construct L, the equations of motion can be obtained using the Euler-Lagrange equations and the null constraint $g_{\mu\nu} p^\mu p^\nu = 0$:

$$dt/d\lambda = A^{-2}\varepsilon f^{-b/a}, \qquad (18a)$$

$$(d\rho/d\lambda)^2 = A^{-4}\left[c^2\varepsilon^2 - (h/\rho)^2 f^{2b/a-1}\right], \qquad (18b)$$

$$d\theta/d\lambda = 0, \qquad (18c)$$

$$d\psi/d\lambda = A^{-2}(h/\rho^2) f^{b/a-1}. \qquad (18d)$$

where ε and h are constants of motion, associated with energy and angular momentum respectively. Combining Eqs. (18a) and (18b) we obtain:

$$d\psi/d\rho = \rho^{-2} f^{b/a-1}\left[\sigma^{-2} - \rho^{-2} f^{2b/a-1}\right]^{-1/2} \qquad (19)$$

where $\sigma \equiv h/(\varepsilon c)$ is the impact parameter.

Let us now solve for the angle ψ in integral form. The impact parameter can be eliminated in favor of α by noticing that the angle between p^ψ and p^ρ at $\rho = \rho_s$ is $\tan\alpha = [p^\psi p_\psi/(p^\rho p_\rho)]^{1/2}$ [88] (see Fig. 4). Using Eqs. (18b) and (18d), we find

$$\sin\alpha = (\sigma/\rho_s)(1 - \bar{a}_s)^{b/a-1/2}, \qquad (20)$$

which in turn results in

$$\psi = \sin\alpha \int_0^1 dy\, (1 - \bar{a}_s y)^{b/a-1}$$
$$\times \left[(1 - \bar{a}_s)^{2b/a-1} - y^2 \sin^2\alpha\,(1 - \bar{a}_s y)^{2b/a-1}\right]^{-1/2}. \quad (21)$$

where we have defined $y \equiv \rho_s/\rho$.

This integral has a singularity whenever $\sin\alpha = 1$ and $y \to 1$. The singularity is power-law integrable and can be removed introducing the new variable $x = \sqrt{1 - y}$ [43, 89]. In terms of x, we obtain

$$\psi = 2\sin\alpha \int_0^1 dx\, x\, [1 - \bar{a}_s(1 - x^2)]^{b/a-1}$$
$$\times \left\{(1 - \bar{a}_s)^{2b/a-1}\right.$$
$$\left. - (1 - x^2)^2 \left[1 - \bar{a}_s(1 - x^2)\right]^{2b/a-1} \sin^2\alpha\right\}^{-1/2}. \quad (22)$$

In the General Relativity limit ($a/b = 1$), this result agrees with the literature [42, 43, 75]. In the Newtonian limit ($a_s = 0$), $\psi = \alpha$ and the bending angle $\beta \equiv \psi - \alpha$ (cf. Fig. 4) is zero.

Figure 5 shows ψ calculated in the range $\alpha \in [0, \pi/2]$, for the stellar models in Table I. In the general relativistic limit
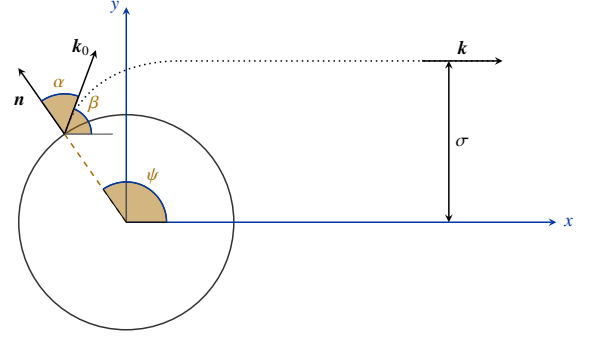

FIG. 4. Bird's eye view of the rotating neutron star. The photon is emitted along a unit vector $\boldsymbol{k}_0$ with an angle α with respect to a normal unit vector $\boldsymbol{n}$, from a small hotspot located at ψ with respect to the line of sight. The star's gravitational field changes the photon trajectory by a bending angle $\beta \equiv \psi - \alpha$, seen to arrive with an impact parameter σ along the unit vector $\boldsymbol{k}$.

($Q = 0$ or $a/b = 1$) our results agree with [75]. A nonzero scalar charge has the effect of increasing/decreasing $\cos\psi$ relative to General Relativity depending on whether the conformal factor at the stellar surface is smaller/larger than unity. This enhancement/suppression is a manifestation of spacetime becoming compressed/stretched in the star's vicinity in scalar-tensor gravity because of the conformal factor. This effect is more salient as $\alpha \to \pi/2$ and is virtually negligible for small α.

C. Visible fraction of the star and visibility conditions

The light ray that defines the star's visible area is the one emitted at an angle $\alpha = \pi/2$ (i.e. tangent to a vector normal to the surface) from a position specified by an angle ψ, measured with respect to the line of sight of the observer (cf. Fig. 4). In flat spacetime, this means that the visibility condition is

$$\cos\psi > 0. \qquad \text{flat spacetime} \qquad (23)$$

Due to light bending, however, we can see more than half of a spherically symmetric neutron star, i.e. a photon emitted with $\cos\psi < 0$ can reach the observer at spatial infinity. However, there is a critical value

$$\cos\psi_c < 0, \qquad \text{curved spacetime} \qquad (24)$$

which determines the last visible ring of the star. The hotspot is visible if

$$\cos\psi > \cos\psi_c. \qquad \text{visibility condition} \qquad (25)$$

This value can be calculated numerically using Eq. (22) with $\alpha = \pi/2$, i.e. $\psi_c \equiv \psi(\alpha = \pi/2)$.

We define the visible fraction of the surface as the ratio:

$$\delta f \equiv \frac{A_s^2 \rho_s^2 (1 - \bar{a}_s)^{1-b/a} \int_0^{\psi_c} \int_0^{2\pi} d\psi'\, d\phi\, \sin\psi'}{4\pi A_s^2 \rho_s^2 (1 - \bar{a}_s)^{1-b/a}}$$
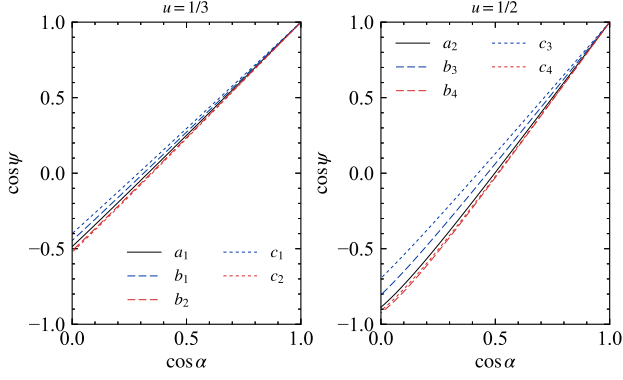$$= \frac{1 - \cos\psi_c}{2}. \qquad (26)$$

FIG. 5. Effect of the scalar charge on ψ as a function of α. The scalar charge affects ψ mostly at $\alpha \approx \pi/2$, while for $\alpha \approx 0$ its influence is negligible.

FIG. 6. Effect of the scalar charge on the time-delay of photons as they escape the neutron star. As in the case of the angle ψ, the effect is largest when α approaches $\pi/2$, while it is negligible as $a \to 0$.

In the Newtonian limit, $\psi_c = \pi/2$ and $\delta f = 1/2$, i.e. half of the star is visible as expected. For relativistic stars, this number increases since $\cos \psi_c < 0$ in general, as shown in Fig. 5. As we have seen in scalar-tensor gravity, this effect can become larger or smaller in comparison to General Relativity depending on whether the conformal factor at the stellar surface is smaller or larger than unity. For instance, when $u = 0.5$, $\delta f \approx 0.94$ in General Relativity (model a_2 in Table I), while it becomes $\delta f \approx 0.85, 0.95$ in scalar-tensor gravity for $A_s = 0.9, 1.1$ and large $Q = 1$ (models c_3 and c_4 in Table I).

The above considerations implicitly assume that the light ring of the star is inside the stellar radius. When this is the case, tangential photons (ie. those emitted with $\alpha = \pi/2$) do escape to spatial infinity. However, if the light ring is outside of the stellar surface, then tangential photons will not escape to spatial infinity. Instead, there will be some maximum α for which photons do reach the observer, and this maximum angle will now need to be used to define the visible fraction of the star. In this paper, however, for all the stellar models we consider, the light ring is inside of the stellar surface, and thus, the analysis of the visible fraction presented above apply.

D. Photon time-delay

Just as curvature deflects photons around the star, it also slows them down through the Shapiro time delay effect. The magnitude of this effect can be calculated using Eqs. (18a) and (18b), which gives

$$t = (1/c) \int_{\rho_s}^{\infty} d\rho \, f^{-b/a} \left[1 - (\sigma/\rho)^2 f^{2b/a-1} \right]^{-1/2}, \qquad (27)$$

and from which we define the time delay as

$$\Delta t \equiv t(\sigma) - t(\sigma = 0), \qquad (28)$$

defined with respect to a photon emitted directly towards the observer (i.e. zero impact parameter $\sigma = 0$). As in the case
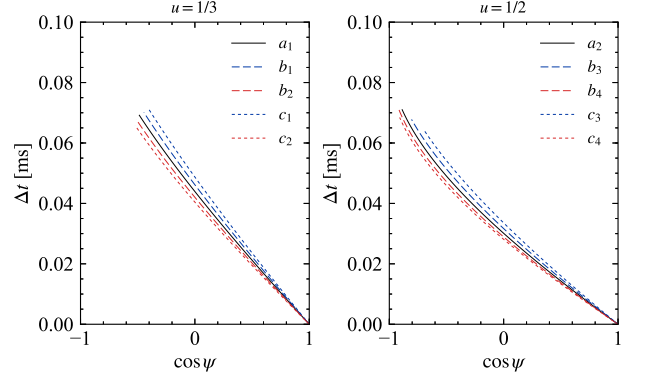
for ψ, we can write the time delay integral in terms of the emission angle $\sin \alpha$ and introduce the same integration variables $\rho_s/\rho = y = 1 - x^2$, with the latter to remove (again) a singularity. The final expression becomes:

$$\Delta t = (2\rho_s/c) \int_0^1 dx \, x \, [1 - \bar{a}_s(1 - x^2)]^{-b/a} (1 - x^2)^{-2}$$
$$\times \left[\!\left[\left\{ 1 - (1 - x^2)^2 (1 - \bar{a}_s)^{1-2b/a} \right. \right.$$
$$\left. \left. \times \left[1 - \bar{a}_s(1 - x^2) \right]^{2b/a-1} \sin^2 \alpha \right\}^{-1/2} - 1 \right]\!\right], \qquad (29)$$

which reduces to the general relativistic expression when $a/b = 1$ or $Q = 0$ [43].

Figure 6 shows the time-delay Δt as a function of angle ψ. Our results agree with [75] in the limit $a/b = 1$ (or $Q = 0$). In scalar-tensor theory, this delay is weakly dependent on the mass, as also observed in General Relativity by [75], having a maximum value of $\Delta t \approx 0.07$ ms irrespective of the Q. The deviations from General Relativity increase for larger values of Q. Similarly to the calculation of ψ, this increase is largest when $\psi \to \pi/2$.

E. The bolometric flux in scalar-tensor gravity

We now combine the results from the previous sections and construct the pulse profile equation in the Just spacetime, following closely [42, 43, 46, 75].

Before jumping into the calculation of the bolometric flux, let us define some more geometrical quantities that will be useful in the calculation. Consider the radial unit vector $\boldsymbol{n}$ at the location of the hotspot and the unit vector $\boldsymbol{k}$ along the line of sight (cf. Fig 3). Since the angle ψ is defined between $\boldsymbol{n}$ and the line of sight, we have

$$\cos \psi = \boldsymbol{k} \cdot \boldsymbol{n}. \qquad (30)$$

Due to the rotation, $(\boldsymbol{k} \cdot \boldsymbol{n})$ varies periodically

$$\cos \psi = \cos \iota_o \cos \theta_s + \sin \iota_o \sin \theta_s \cos \phi_s, \qquad (31)$$

where ι_o is the angle between the line of sight with respect to the spin axis, θ_s is the spot's colatitude and $\phi_s = 2\pi\nu t$ is the rotational phase of the spot. We choose $t = 0$ to correspond to when the spot is closest to the observer.

The angle ψ measures the *apparent* inclination of the spot relative to the line of sight, but due to light-bending this is different from the true inclination. To define the latter, recall that $\boldsymbol{k}_0$ is the unit vector in the direction in which the photon is emitted, such that the emission angle α is then

$$\cos\alpha = \boldsymbol{k}_0 \cdot \boldsymbol{n}. \tag{32}$$

Due to special relativistic aberration, an observer comoving with the hotspot measures an angle α'. The angles α and α' are related by [42]

$$\cos\alpha' = \delta\cos\alpha, \tag{33}$$

where δ is the Doppler factor

$$\delta = [\gamma(\theta_s)(1 - \beta\cos\xi)]^{-1}. \tag{34}$$

Here, $\gamma(\theta_s) = (1 - \beta^2)^{-1/2}$ is the Lorentz factor and $\beta = v/c$ is the spot's velocity, which satisfies

$$\beta = \frac{2\pi\rho_s}{c}\frac{\nu}{(1 - \bar{a}_s)^{b/(2a)}}\sin\theta_s. \tag{35}$$

where we corrected the rotation frequency by the redshift factor

$$\nu/\nu_0 = \sqrt{g_{tt}(\rho_s)/g_{tt}(\infty)} = A_s(1 - \bar{a}_s)^{b/(2a)}. \tag{36}$$

The angle between $\boldsymbol{k}_0$ and the spot velocity vector $\boldsymbol{\beta}$ is denoted by ξ (see Fig. 3), and it is related to the other angles via [75]:

$$\cos\xi = (\boldsymbol{\beta}\cdot\boldsymbol{k}_0)/\beta = -(\sin\alpha/\sin\psi_s)\sin\iota_o\sin\phi_s \tag{37}$$

With this at hand, let us now return to the observed flux from the spot at energy E. This quantity can be defined as

$$dF_E = I(E, \alpha)d\Omega, \tag{38}$$

where $I(E, \alpha)$ is the specific intensity of radiation at infinity and $d\Omega$ is the solid angle on the observer's sky occupied by the spot with differential area dS' measured in a comoving reference frame. Let us determine $I(E, \alpha)$ and $d\Omega$ separately, starting with the latter.

The solid angle can be written in terms of the impact parameter σ as

$$d\Omega = (\sigma\, d\sigma\, d\varphi)/D^2, \tag{39}$$

where D is the distance to the source and φ is the azimuthal angle around the vector $\boldsymbol{k}$ (not to be confused with the scalar field). In terms of the surface area [cf. Eq. (8)]

$$dA = A_s^2\rho_s^2(1 - \bar{a}_s)^{1-b/a}\sin\psi d\psi d\varphi, \tag{40}$$

we have

$$d\Omega = \frac{\sigma}{A_s^2\rho_s^2}\frac{(1 - \bar{a}_s)^{b/a-1}}{\sin\psi}\frac{d\sigma}{d\psi}\frac{dA}{D^2}. \tag{41}$$

Using that the spot area projected onto the plane perpendicular to the photon propagation direction is a Lorentz invariant, we have

$$dA'\cos\alpha' = dA\cos\alpha, \tag{42}$$

where dA' (dA) is the differential spot area measured by a comoving (static) reference frame. We can now write the solid angle as

$$d\Omega = \frac{\sigma}{A_s^2\rho_s^2}\frac{(1 - \bar{a}_s)^{b/a-1}}{\sin\psi}\frac{d\sigma}{d\psi}\frac{\cos\alpha'}{\cos\alpha}\frac{dA'}{D^2}, \tag{43}$$

where dA' [written (θ, ϕ) coordinates] is

$$dA' = \gamma(\theta)A_s^2\rho_s^2(1 - \bar{a}_s)^{1-b/a}\sin\theta d\theta d\phi, \tag{44}$$

where we took into account a factor of $\gamma(\theta)$ relating dA and dA'. This term is due to Lorentz contraction of the linear differential interval correspondent to an angular interval $d\phi$ measured in the static reference frame [46, 87].

Finally, using Eq. (20) for the impact parameter and remembering that α depends implicitly on ψ [cf. Eq. (22)] we find:

$$d\sigma/d\psi = \rho_s(1 - \bar{a}_s)^{1/2-b/a}(d\sin\alpha/d\psi), \tag{45}$$

which substituted back into Eq. (43) gives our final expression for $d\Omega$:

$$d\Omega = (1 - \bar{a}_s)^{-b/a}\cos\alpha'\frac{d\cos\alpha}{d\cos\psi}\frac{dA'}{A_s^2D^2}. \tag{46}$$

Now we turn our attention to the specific intensity. We assume it can be decomposed (in the comoving reference frame) as [43]

$$I'_0(E'_0, \alpha') = g'(\alpha')f'(E'_0), \tag{47}$$

where $g'(\alpha')$ and $f'(E'_0)$ are respectively a beaming and a spectral function, and E'_0 is the photon energy measured by the comoving observer at the stellar surface. In general, the specific intensity has a dependence on α' due to Thompson scattering as the photon propagates through the star's atmosphere [43, 90].

In order to express the specific intensity in terms of quantities measured by an observer far away from the star, we proceed in two steps. First, we Lorentz transform the energy E'_0 measured by a comoving reference frame at the stellar surface to the energy E_0 measured by a static reference frame near the stellar surface via

$$E_0 = \delta E'_0. \tag{48}$$

The ratio (specific intensity/energy^3) is a Lorentz invariant allowing us to write

$$I_0(E_0, \alpha)/E_0^3 = I'_0(E'_0, \alpha')/E_0'^3. \tag{49}$$

We now transform E_0 to the energy E measured by the distant observer. These energies are related by a gravitational redshift factor

$$E = A_s(1 - \bar{a}_s)^{b/(2a)}E_0. \tag{50}$$

Consequently, our final result becomes:

$$I(E, \alpha) = A_s^3 \delta^3 (1 - \bar{a}_s)^{3b/(2a)} I_0'(E_0', \alpha'), \qquad (51)$$

which relates the specific intensity as measured by a comoving observer at the stellar surface to that measured by a distant observer, including both special and general relativistic effects.

Substituting Eqs. (46) and (51) into Eq. (38) we obtain

$$dF_E = A_s (1 - \bar{a}_s)^{b/(2a)} \delta^3 I_0'(E_0', \alpha') \cos \alpha' \frac{d \cos \alpha}{d \cos \psi} \frac{dA'}{D^2}. \quad (52)$$

To obtain the bolometric flux, we integrate Eq. (52) over energies E. Using one last time the relation between E and E_0' [i.e. using Eqs. (48) and (50)] we find

$$\begin{aligned} dF &\equiv \int dE \, dF_E, \\ &= A_s^2 (1 - \bar{a}_s)^{b/a} \delta^4 \cos \alpha' \frac{d \cos \alpha}{d\psi} \frac{dA'}{D^2} \int dE_0' \, I_0'(E_0', \alpha'), \\ &= A_s^2 (1 - \bar{a}_s)^{b/a} \delta^4 \cos \alpha' \frac{d \cos \alpha}{d \cos \psi} \frac{dA'}{D^2} I_0'(\alpha'). \quad (53) \end{aligned}$$

As a final step, we can reexpress the angle α' (measured by a comoving reference frame at the stellar surface) in terms of α (measured by a reference frame static near the star) using Eq. (33). Our final expression for the bolometric flux measured by an observer due to radiation emission by a small element dS' of the hotspot is

$$dF = A_s^2 (1 - \bar{a}_s)^{b/a} \delta^5 \cos \alpha \frac{d \cos \alpha}{d \cos \psi} \frac{dA'}{D^2} I_0'(\alpha'). \quad (54)$$

This formula is the main result of this paper. It is sufficiently general to describe the Jordan-frame bolometric flux of a static, spherically symmetric star whose exterior spacetime is described by the Just metric, including special relativistic effects (aberration and Doppler boosts) and gravitational redshift.

For simplicity, let us assume that the specific intensity is isotropic (independent of α') and that the hotspot is small in size. Writing $I_0(\alpha') = I_0'$, normalizing the flux dF by $I_0' dA'/D^2$ we have[4].

$$F = A_s^2 (1 - \bar{a}_s)^{b/a} \delta^5 \cos \alpha \frac{d \cos \alpha}{d \cos \psi}, \qquad (55)$$

which is our final result, used in Sec. IV.

When two antipodal hotspots are present, the total flux is obtained as (see Fig. 3)

$$F = F(\iota_o, \pi - \theta_s, \pi + \phi_s, \bar{a}_s, \bar{b}_s) + F(\iota_o, \theta_s, \phi_s, \bar{a}_s, \bar{b}_s). \quad (56)$$

---

[4] For hotspots of large angular radius, the flux must be calculated by a discretization of the area occupied by the spot on a grid (θ_i, ϕ_i), with each cell having a corresponding Lorentz factor $\gamma(\theta_i)$, see Eq. (44) [43, 46]

The hotspot is visible for the distant observer when $\cos \psi > \cos \psi_c$. For the antipodal hotspot the visibility condition is when $\cos \psi > -\cos \psi_c$ [75].

Let us comment on some of the features of Eq. (55). First, the general form of the expression is analogous to the one found in [75] and agrees with it in the general relativistic limit $a/b = 1$. The prefactor $1 - \bar{a}_s$ reduces the peak-to-peak amplitude of the pulse's profile in comparison to the Newtonian result (in which $\bar{a}_s \to 0$). Second, the Doppler factor δ^5 oscillates with time, skewing the otherwise sinusoidal pulse profile.

IV. NUMERICAL MODELING AND PULSE PROFILES IN SCALAR-TENSOR THEORY

Having determined the expression for the radiation flux, let us outline how the pulse profiles are numerically calculated. The steps are:

(i) From Eq. (31) we determine ψ at a given phase ϕ_s.

(ii) With ψ at hand, we check whether or not the spot is visible. If $\cos \psi > \cos \psi_c$, the spot is visible and we proceed with the remaining steps. Otherwise, the flux is zero.

(iii) With ψ at hand, we then determine α, inverting Eq. (22). This is done numerically with the shooting method.

(iv) Knowing α, we can calculate the derivative $(d \cos \alpha / d \cos \psi)$ for the current value of ψ. In practice, it is easier to determine $(d \cos \psi / d \cos \alpha)^{-1}$ and evaluate it at the value of α found in step (iii). To do so, we first calculate $\cos \psi$ on a fine grid $\cos \alpha \in [0, 1]$, interpolate the data using a spline interpolation, and from this we calculate the derivative numerically.

(v) We calculate the Lorentz and Doppler factors in Eq. (34), and the time-delay in Eq. (29).

(vi) We combine all these ingredients in Eq. (55) to obtain the flux. Finally, we correct the phase due to time-delay by adding $(2\pi\nu\Delta t)$ to ϕ_s.

Let us now show some numerical results for one hotspot with our catalog of stellar models (see Table I). As described in Sec. I, these profiles could represent observations from burst oscillations of an accreting neutron star. We consider two illustrative situations, one in which $\theta_s = \iota_o = 45°$ (as in [75]), and another with $\theta_s = \iota_o = 90°$ (as in [43]) to illustrate the general effects of a nonzero scalar charge on the pulse profile. In the former case, our results agree with those presented in [75] in the limit of General Relativity (modulo a different normalization). To make the effects of scalar-tensor gravity more clearly visible, we consider extreme stellar models, with $u = 0.5$ and rotation frequency of $\nu = 600$ Hz. With these choices the strong-gravity effects on the waveform become more pronounced in both figures. To avoid excessive clutter in the panels and complement the sample pulse profile shown in Fig. 1 we use only the models with $A_s > 1$ (i.e. b_4

and c_4). The waveforms for b_3 and c_3 are similar to that shown in Fig. 1. same compactness.

Figure 7 studies the $\theta_s = \iota_o = 45°$ case, showing the pulse profile in a number of special cases. The top-left panel considers slowly-rotating stars, whose pulse profile is calculated setting the Doppler and Lorentz factors to unity and neglecting the travel time delay of photons [cf. Eq. (55)]. The top-right (bottom-left) panel shows how the pulse profile changes when we include Doppler effects (and time-delay). The Doppler factor changes the amplitude of the waveform and its overall shape by skewing it. A time-delay has the effect of shifting the arrival time of the pulse (non-uniformly over the course of a revolution), resulting in an additional small deformation of the waveform. Overall, the impact of each of these effects in scalar-tensor gravity is identical to that in General Relativity [75], the difference being the magnitude of these effects. This is not surprising given that the flux formula in Eq. (55) has the same functional form in scalar-tensor gravity as in General Relativity.

Figure 8 studies the $\theta_s = \iota_o = 90°$ case. The same conclusions drawn from Fig. 7 are applicable here. Because of the geometrical arrangement of the hotspot's location and the line of sight of the observer, the hotspot becomes invisible to the observer during certain phase intervals. These intervals when the hotspot is not visible depend on the values of Q in scalar-tensor theory, and thus, they could provide yet another telltale sign of a deviation from General Relativity. Of course, other stellar parameters, like the inclination angle, also affect the occultation period; thus, a full covariance analysis is necessary to determine the detectability of this effect.

V. CONCLUSIONS AND OUTLOOK

We introduced a Just-Doppler approximation for calculating pulse profiles of rotating neutron stars in scalar-tensor gravity. The main result, encapsulated in Eq. (54), allows one to calculate the waveforms, including effects of the strong-gravity and special relativistic effects, generalizing the Schwarzschild plus Doppler approximation to scalar-tensor theories of gravity. We presented a selection of sample results for burst oscillation waveforms of an infinitesimal hotspot and discussed the implications of the presence of a nonzero scalar charge on it.

The model-independent character of the formalism opens the possibility of constraining a large class of scalar-tensor gravity models with upcoming x-ray timing data releases from NICER. In this regard, our work is close in spirit to [65], except that that work focused on binary pulsars. In a forthcoming paper, we will present a statistical likelihood analysis discussing the strength of potential future constraints on scalar-tensor gravity with pulse profile observations. We emphasize, however, that whether future constraints can be placed on scalar-tensor gravity with NICER data will require a full data analysis study that varies over all model parameters in the presence of noise; such a study is now possible thanks to the pulse-profile model presented here, and it will be carried out in the future.

Despite the generality of the present formalism, it is necessary to discuss its limitations and signal in which directions it can be improved further. At considerably large rotational frequencies ($\nu \gtrsim 300$ Hz), the Schwarzschild-Doppler approximation becomes inappropriate as discussed, e.g. in [84], because of the rotation-induced quadrupolar deformation of star. To include this effect in the pulse profiles, one must first extend the Just metric to rotating stars. To leading-order in rotation, that is, including only frame-dragging effects while keeping a spherical geometry for the star, this calculation was done in [91]. Using the Hartle-Thorne perturbative expansion, Berti and Pani [63] extended this work to second-order in rotation, which includes the quadrupolar deformation of the star. Alternatively, one could also work entirely numerically and carry out ray-tracing calculations (as in [83, 84, 86, 87]), evolving the photon geodesics in a numerically constructed spacetime for rotating neutron stars in scalar-tensor gravity [92]. A caveat of this numerical approach is that the spacetime can only be determined numerically *after* choosing a particular conformal factor $A(\varphi)$ *and* the equation of state, therefore inevitably making it model-dependent.

Another approach would be to follow the work in [33, 93, 94] and use the Ernst formalism to obtain an axisymmetric spacetime in Weyl-Papapetrou coordinates in terms of an multipolar expansions of the multipole moments of the rotating neutron star and the scalar field. The multipole moments appear as free constants in the spacetime metric, thus allowing one to develop an extension of the model-independent pulse profile model introduced here. In this approach, and as an intermediate step, one would first have to *estimate* numerically the values of these moments in order to have an analytic spacetime that describes accurately the one constructed numerically, for example in [92].

We emphasize, however, that Cadeau et al. [84] have shown that even in the presence of stellar oblateness, the Schwarzschild-Doppler approximation works quite well at these frequencies when θ_s and ι_o are *near the equator* as in the case of Fig. 8. Geometrically, this is due to the small difference between the normal vector $\boldsymbol{n}$ on a spherical and a oblate surface near the equator, which suppresses the effect of the star's oblateness. Because of the purely geometrical nature of this argument, we expect the Just-Doppler approximation to accurately describe the pulse profile when $\theta_s \approx \iota_o \approx 90°$ even for rapidly-rotating neutron stars in scalar-tensor gravity.

Finally, it could also be interesting to consider other theories of gravity or to use a parametrized framework – to consider model-independent deformations of the Tolman-Oppenheimer-Volkoff equations and the Schwarzschild spacetime – as introduced in [26, 30]. Work in all of these directions is currently underway and will be reported in several future publications.
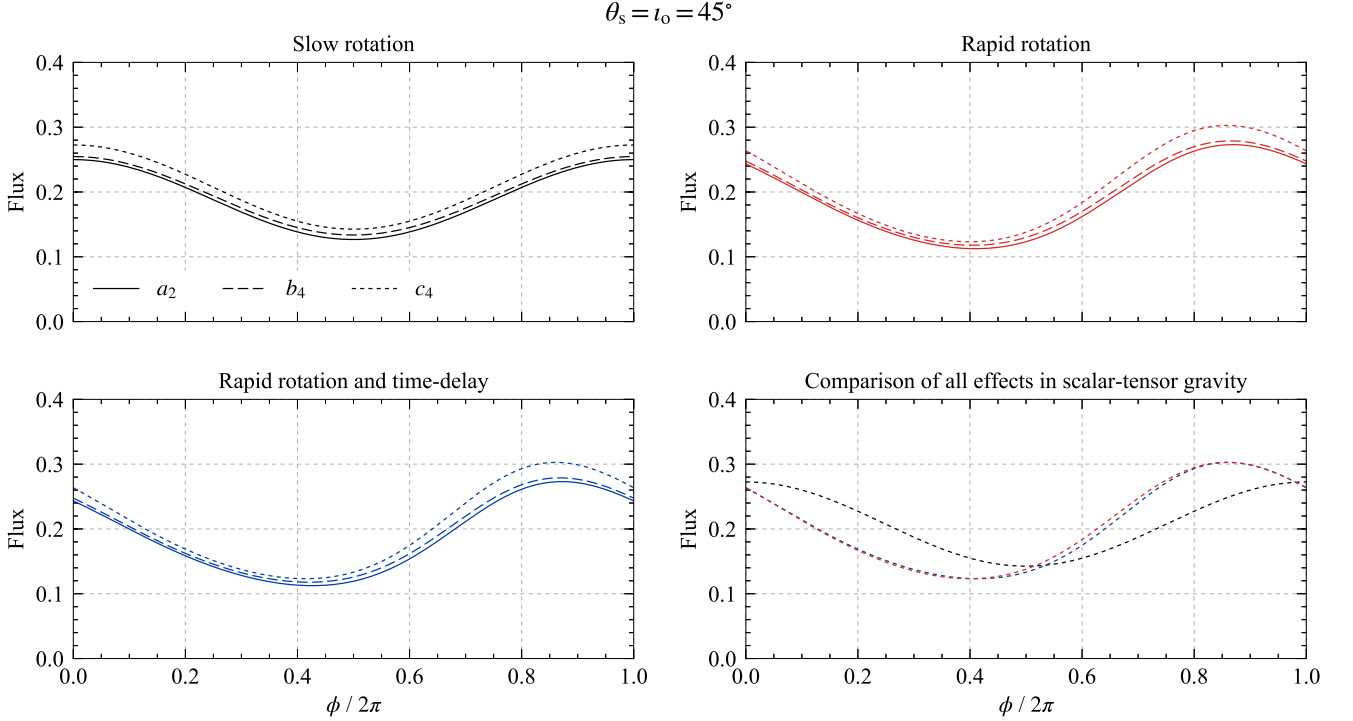
$$\theta_s = \iota_o = 45°$$

FIG. 7. We illustrate the effects of a nonzero scalar charge on the pulse profile for one hotspot. We choose $\theta_s = \iota_o = 45°$ and stars with $u = 0.5$ and increasing values of scalar charge-to-mass ration Q (models a_2, b_4 and c_4 in Table I, where recall a_2 is the general relativistic limit). We show slowly-rotating stars ($\delta = 1$, $\Delta t = 0$) in the top-left panel, rapidly-rotating stars neglecting time-delay effects ($\delta \neq 1$, $\Delta t = 0$) in the top-right panel, and including them ($\delta \neq 1$, $\Delta t \neq 0$) in the bottom-left panel. In the last panel (bottom-right), we compare the pulse profile in these three situations for a star with $Q = 1$ and $u = 0.5$ (model c_4 in Table I).

Appendix A: Existence and location of a light ring in the Just spacetime

In this appendix we obtain the location for the light ring in the Just spacetime, following closely the presentation of [74]. Consider the $(d\psi/d\rho)$ equation squared:

$$(d\psi/d\rho)^2 = \rho^{-4} f^{2b/a-2} (\sigma^{-2} - \rho^{-2} f^{2b/a-1})^{-1}. \quad (A1)$$

Writing $(d\rho/d\psi)^2$ instead:

$$(d\rho/d\psi)^2 = \rho^4 f^{-2b/a+2} (\sigma^{-2} - \rho^{-2} f^{2b/a-1}). \quad (A2)$$

which can be rearranged as:

$$[\rho^{-2} (d\rho/d\psi)]^2 f^{2b/a-2} = \sigma^{-2} - \rho^{-2} f^{2b/a-1}. \quad (A3)$$

The left-hand side is positive, so we must have

$$\sigma^{-2} - \rho^{-2} f^{2b/a-1} \geq 0 \quad (A4)$$

The second term has an extrema at some ρ_c for which:

$$d(\rho^{-2} f^{2b/a-1})/d\rho = 0. \quad (A5)$$

Taking the derivative, we find that it occurs at

$$\rho_c = \frac{1}{2}(a + 2b). \quad (A6)$$

In the general relativistic limit, we have that $a = 2Gm/c^2 = b$, and we recover the usual location of the light ring in the Schwarzschild spacetime, i.e. $3GM/c^2$.

In the Just metric, for the light ring to be within the star, the star's radius ρ_s must satisfy:

$$\rho_s \geq \frac{1}{2}(a + 2b) = \frac{G_* m}{c^2}(2 + \sqrt{1 + Q^2}) \quad (A7)$$

Equivalent expressions can be obtained dividing the inequality by ρ_s and with a few rearrangements:

$$\bar{a}_s \leq 2(1 - \bar{b}_s), \quad (\bar{b}_s/2)(2 + \sqrt{1 + Q^2}) \leq 1. \quad (A8)$$

These equalities are shown in Fig. 2 by the dot-dashed lines.
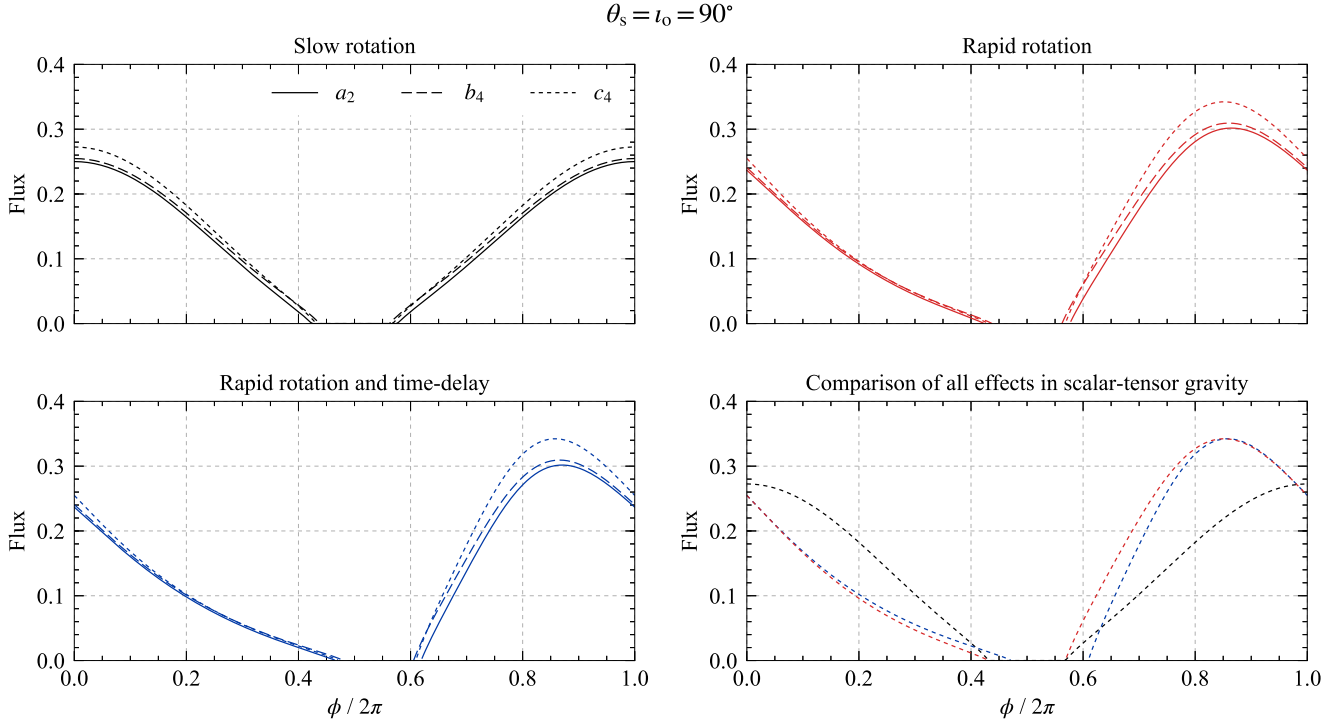
$$\theta_s = \iota_o = 90°$$

FIG. 8. Similar to Fig. 7, but for $\theta_s = \iota_o = 90°$. Due to the geometrical configuration of the hot spot and the observer, the flux hot spot becomes invisible momentarily as the star rotates. Observe that where the flux disappears depends on the value of Q.

[1] J. M. Lattimer and M. Prakash, Phys. Rept. **621**, 127 (2016), arXiv:1512.07820 [astro-ph.SR].

[2] C. M. Will, Living Rev. Rel. **17**, 4 (2014), arXiv:1403.7377 [gr-qc].

[3] T. Baker, D. Psaltis, and C. Skordis, Astrophys. J. **802**, 63 (2015), arXiv:1412.3455 [astro-ph.CO].

[4] L. Bonolis, Eur. Phys. J. **H42**, 311 (2017), arXiv:1703.09991 [physics.hist-ph].

[5] B. P. Abbott *et al.* (Virgo, LIGO Scientific), Phys. Rev. Lett. **116**, 061102 (2016), arXiv:1602.03837 [gr-qc].

[6] B. P. Abbott *et al.* (Virgo, LIGO Scientific), Phys. Rev. Lett. **116**, 221101 (2016), arXiv:1602.03841 [gr-qc].

[7] T. Clifton, P. G. Ferreira, A. Padilla, and C. Skordis, Phys. Rept. **513**, 1 (2012), arXiv:1106.2476 [astro-ph.CO].

[8] E. Berti *et al.*, Class. Quant. Grav. **32**, 243001 (2015), arXiv:1501.07274 [gr-qc].

[9] S. Alexander and N. Yunes, Phys. Rept. **480**, 1 (2009), arXiv:0907.2562 [hep-th].

[10] A. G. Riess *et al.* (Supernova Search Team), Astron. J. **116**, 1009 (1998), arXiv:astro-ph/9805201 [astro-ph].

[11] S. Perlmutter *et al.* (Supernova Cosmology Project), Astrophys. J. **517**, 565 (1999), arXiv:astro-ph/9812133 [astro-ph].

[12] Y. Sofue and V. Rubin, Ann. Rev. Astron. Astrophys. **39**, 137 (2001), arXiv:astro-ph/0010594 [astro-ph].

[13] G. Bertone and D. Hooper, (2016), arXiv:1605.04909 [astro-ph.CO].

[14] D. N. Spergel *et al.* (WMAP), Astrophys. J. Suppl. **148**, 175 (2003), arXiv:astro-ph/0302209 [astro-ph].

[15] L. Canetti, M. Drewes, and M. Shaposhnikov, New J. Phys. **14**, 095012 (2012), arXiv:1204.4186 [hep-ph].

[16] T. Damour, in *6th SIGRAV Graduate School in Contemporary Relativity and Gravitational Physics: A Century from Einstein Relativity: Probing Gravity Theories in Binary Systems Villa Olmo, Como, Italy, May 17-21, 2005* (2007) arXiv:0704.0749 [gr-qc].

[17] N. Wex, (2014), arXiv:1402.5594 [gr-qc].

[18] M. Kramer, Int. J. Mod. Phys. **D25**, 1630029 (2016), arXiv:1606.03843 [astro-ph.HE].

[19] A. M. Archibald, N. V. Gusinskaia, J. W. T. Hessels, A. T. Deller, D. L. Kaplan, D. R. Lorimer, R. S. Lynch, S. M. Ransom, and I. H. Stairs, (2018), 10.1038/s41586-018-0265-1, [Nature559,73(2018)], arXiv:1807.02059 [astro-ph.HE].

[20] B. Abbott *et al.* (Virgo, LIGO Scientific), Phys. Rev. Lett. **119**, 161101 (2017), arXiv:1710.05832 [gr-qc].

[21] J. Sakstein and B. Jain, Phys. Rev. Lett. **119**, 251303 (2017), arXiv:1710.05893 [astro-ph.CO].

[22] T. Baker, E. Bellini, P. G. Ferreira, M. Lagos, J. Noller, and I. Sawicki, Phys. Rev. Lett. **119**, 251301 (2017), arXiv:1710.06394 [astro-ph.CO].

[23] J. M. Ezquiaga and M. Zumalacárregui, Phys. Rev. Lett. **119**, 251304 (2017), arXiv:1710.05901 [astro-ph.CO].

[24] P. Creminelli and F. Vernizzi, Phys. Rev. Lett. **119**, 251302 (2017), arXiv:1710.05877 [astro-ph.CO].

[25] D. Bettoni, J. M. Ezquiaga, K. Hinterbichler, and M. Zumalacárregui, Phys. Rev. **D95**, 084029 (2017), arXiv:1608.01982 [gr-qc].

[26] K. Glampedakis, G. Pappas, H. O. Silva, and E. Berti, Phys. Rev. **D92**, 024056 (2015), arXiv:1504.02455 [gr-qc].

[27] D. Psaltis, Living Rev. Rel. **11**, 9 (2008), arXiv:0806.1531 [astro-ph].

[28] S. DeDeo and D. Psaltis, Phys. Rev. Lett. **90**, 141101 (2003), arXiv:astro-ph/0302095 [astro-ph].

[29] D. Psaltis, Phys. Rev. **D77**, 064006 (2008), arXiv:0704.2426 [astro-ph].

[30] K. Glampedakis, G. Pappas, H. O. Silva, and E. Berti, Phys. Rev. **D94**, 044030 (2016), arXiv:1606.05106 [gr-qc].

[31] S. DeDeo and D. Psaltis, Submitted to: Phys. Rev. D (2004), arXiv:astro-ph/0405067 [astro-ph].

[32] D. D. Doneva, S. S. Yazadjiev, N. Stergioulas, K. D. Kokkotas, and T. M. Athanasiadis, Phys. Rev. **D90**, 044004 (2014), arXiv:1405.6976 [astro-ph.HE].

[33] G. Pappas and T. P. Sotiriou, Mon. Not. Roy. Astron. Soc. **453**, 2862 (2015), arXiv:1505.02882 [gr-qc].

[34] Z. Arzoumanian et al., (2009), arXiv:0902.3264 [astro-ph.HE].

[35] J. Poutanen, AIP Conf. Proc. **1068**, 77 (2008), arXiv:0809.2400 [astro-ph].

[36] F. Özel, Rept. Prog. Phys. **76**, 016901 (2013), arXiv:1210.0916 [astro-ph.HE].

[37] A. L. Watts et al., Rev. Mod. Phys. **88**, 021001 (2016), arXiv:1602.01081 [astro-ph.HE].

[38] M. C. Miller and F. K. Lamb, Astrophys. J. **499**, L37 (1998), arXiv:astro-ph/9711325 [astro-ph].

[39] N. Weinberg, M. C. Miller, and D. Q. Lamb, Astrophys. J. **546**, 1098 (2001), arXiv:astro-ph/0001544 [astro-ph].

[40] M. P. Muno, F. Özel, and D. Chakrabarty, Astrophys. J. **581**, 550 (2002), arXiv:astro-ph/0204501 [astro-ph].

[41] S. Bogdanov, Astrophys. J. **762**, 96 (2013), arXiv:1211.6113 [astro-ph.HE].

[42] J. Poutanen and M. Gierliński, Mon. Not. Roy. Astron. Soc. **343**, 1301 (2003), arXiv:astro-ph/0303084 [astro-ph].

[43] K. H. Lo, M. C. Miller, S. Bhattacharyya, and F. K. Lamb, Astrophys. J. **776**, 19 (2013), arXiv:1304.2330 [astro-ph.HE].

[44] M. C. Miller and F. K. Lamb, Astrophys. J. **808**, 31 (2015), arXiv:1407.2579 [astro-ph.HE].

[45] A. L. Stevens, J. D. Fiege, D. A. Leahy, and S. M. Morsink, Astrophys. J. **833**, 244 (2016), arXiv:1606.09232 [astro-ph.HE].

[46] K. H. Lo, M. C. Miller, S. Bhattacharyya, and F. K. Lamb, (2018), arXiv:1801.08031 [astro-ph.HE].

[47] T. Salmi, J. Nättilä, and J. Poutanen, Astron. Astrophys. **618**, A161 (2018), arXiv:1805.01149 [astro-ph.HE].

[48] K. C. Gendreau, Z. Arzoumanian, and T. Okajima, in *Space Telescopes and Instrumentation 2012: Ultraviolet to Gamma Ray*, Proc. SPIE, Vol. 8443 (2012) p. 844313.

[49] Z. Arzoumanian et al., in *Space Telescopes and Instrumentation 2014: Ultraviolet to Gamma Ray*, Proc. SPIE, Vol. 9144 (2014) p. 914420.

[50] K. Gendreau and Z. Arzoumanian, Nature Astronomy **1**, 895 (2017).

[51] H. Sotani and U. Miyamoto, Phys. Rev. **D96**, 104018 (2017), arXiv:1710.08581 [astro-ph.HE].

[52] H. Sotani, Phys. Rev. **D96**, 104010 (2017), arXiv:1710.10596 [astro-ph.HE].

[53] T. Chiba, T. Harada, and K.-i. Nakao, Prog. Theor. Phys. Suppl. **128**, 335 (1997).

[54] T. P. Sotiriou, Lect. Notes Phys. **892**, 3 (2015), arXiv:1404.2955 [gr-qc].

[55] T. Damour and G. Esposito-Farèse, Class. Quant. Grav. **9**, 2093 (1992).

[56] H. A. Buchdahl, Phys. Rev. **115**, 1325 (1959).

[57] K. Just, Zeitschrift Naturforschung Teil A **14**, 751 (1959).

[58] R. Coquereaux and G. Esposito-Farèse, Ann. Inst. H. Poincaré Phys. Theor. **52**, 113 (1990).

[59] T. Damour and K. Nordtvedt, Phys. Rev. Lett. **70**, 2217 (1993).

[60] T. Damour and K. Nordtvedt, Phys. Rev. **D48**, 3436 (1993).

[61] D. Anderson, N. Yunes, and E. Barausse, Phys. Rev. **D94**, 104064 (2016), arXiv:1607.08888 [gr-qc].

[62] D. Anderson and N. Yunes, Phys. Rev. **D96**, 064037 (2017), arXiv:1705.06351 [gr-qc].

[63] P. Pani and E. Berti, Phys. Rev. **D90**, 024025 (2014), arXiv:1405.4547 [gr-qc].

[64] M. Minamitsuji and H. O. Silva, Phys. Rev. **D93**, 124041 (2016), arXiv:1604.07742 [gr-qc].

[65] M. W. Horbatsch and C. P. Burgess, Class. Quant. Grav. **29**, 245004 (2012), arXiv:1107.3585 [gr-qc].

[66] C. Palenzuela and S. L. Liebling, Phys. Rev. **D93**, 044009 (2016), arXiv:1510.03471 [gr-qc].

[67] R. F. P. Mendes and N. Ortiz, Phys. Rev. **D93**, 124035 (2016), arXiv:1604.04175 [gr-qc].

[68] H. A. Buchdahl, Phys. Rev. **116**, 1027 (1959).

[69] R. M. Wald, *General Relativity* (Chicago Univ. Pr., Chicago, USA, 1984).

[70] T. Tsuchida, G. Kawamura, and K. Watanabe, Prog. Theor. Phys. **100**, 291 (1998), arXiv:gr-qc/9802049 [gr-qc].

[71] T. P. Sotiriou and V. Faraoni, Phys. Rev. Lett. **108**, 081103 (2012), arXiv:1109.6324 [gr-qc].

[72] F. Özel and P. Freire, Ann. Rev. Astron. Astrophys. **54**, 401 (2016), arXiv:1603.02698 [astro-ph.HE].

[73] M. C. Miller and F. K. Lamb, Eur. Phys. J. **A52**, 63 (2016), arXiv:1604.03894 [astro-ph.HE].

[74] K. R. Pechenick, C. Ftaclas, and J. M. Cohen, ApJ **274**, 846 (1983).

[75] J. Poutanen and A. M. Beloborodov, Mon. Not. Roy. Astron. Soc. **373**, 836 (2006), arXiv:astro-ph/0608663 [astro-ph].

[76] T. Damour and G. Esposito-Farèse, Phys. Rev. Lett. **70**, 2220 (1993).

[77] T. Harada, Prog. Theor. Phys. **98**, 359 (1997), arXiv:gr-qc/9706014 [gr-qc].

[78] H. O. Silva, C. F. B. Macedo, E. Berti, and L. C. B. Crispino, Class. Quant. Grav. **32**, 145008 (2015), arXiv:1411.6286 [gr-qc].

[79] M. Baubock, D. Psaltis, and F. Ã–zel, Astrophys. J. **811**, 144 (2015), arXiv:1505.00780 [astro-ph.HE].

[80] X.-N. Bai and A. Spitkovsky, Astrophys. J. **715**, 1270 (2010), arXiv:0910.5740 [astro-ph.HE].

[81] H. Sotani, Phys. Rev. **D86**, 124036 (2012), arXiv:1211.6986 [astro-ph.HE].

[82] T. M. Braje, R. W. Romani, and K. P. Rauch, Astrophys. J. **531**, 447 (2000), arXiv:astro-ph/0004411 [astro-ph].

[83] C. Cadeau, D. A. Leahy, and S. M. Morsink, Astrophys. J. **618**, 451 (2005), arXiv:astro-ph/0409261 [astro-ph].

[84] C. Cadeau, S. M. Morsink, D. Leahy, and S. S. Campbell, Astrophys. J. **654**, 458 (2007), arXiv:astro-ph/0609325 [astro-ph].

[85] S. M. Morsink, D. A. Leahy, C. Cadeau, and J. Braga, Astrophys. J. **663**, 1244 (2007), arXiv:astro-ph/0703123 [astro-ph].

[86] D. Psaltis and F. Özel, Astrophys. J. **792**, 87 (2014), arXiv:1305.6615 [astro-ph.HE].

[87] J. Nättilä and P. Pihajoki, A&A **615**, A50 (2018), arXiv:1709.07292 [astro-ph.HE].

[88] A. M. Beloborodov, Astrophys. J. **566**, L85 (2002), arXiv:astro-ph/0201117 [astro-ph].

[89] W. H. Press, S. A. Teukolsky, W. T. Vetterling, and B. P. Flannery, *Numerical Recipes 3rd Edition: The Art of Scientific Computing*, 3rd ed. (Cambridge University Press, New York, NY, USA, 2007).

[90] S. Chandrasekhar, *Radiative transfer* (New York: Dover, 1960, 1960).

[91] T. Damour and G. Esposito-Farèse, Phys. Rev. **D54**, 1474 (1996), arXiv:gr-qc/9602056 [gr-qc].

[92] D. D. Doneva, S. S. Yazadjiev, N. Stergioulas, and K. D. Kokkotas, Phys. Rev. **D88**, 084060 (2013), arXiv:1309.0605 [gr-qc].

[93] G. Pappas and T. P. Sotiriou, Phys. Rev. **D91**, 044011 (2015), arXiv:1412.3494 [gr-qc].

[94] G. Pappas, Mon. Not. Roy. Astron. Soc. **466**, 4381 (2017), arXiv:1610.05370 [gr-qc].